Open Dartmouth: Faculty Open Access Articles

6-10-2014

Obscuration by Gas and Dust in Luminous Quasars

S. M. Usman
Johns Hopkins University

S. S. Murray
Johns Hopkins University

R. C. Hickox
Dartmouth College

M. Brodwin
University of Missouri

Follow this and additional works at: https://digitalcommons.dartmouth.edu/facoa

Part of the External Galaxies Commons

Recommended Citation

Usman, S. M.; Murray, S. S.; Hickox, R. C.; and Brodwin, M., "Obscuration by Gas and Dust in Luminous Quasars" (2014). *Open Dartmouth: Faculty Open Access Articles*. 1783.
https://digitalcommons.dartmouth.edu/facoa/1783

OBSCURATION BY GAS AND DUST IN LUMINOUS QUASARS

S. M. Usman[1], S. S. Murray[1,2], R. C. Hickox[3], and M. Brodwin[4]
[1] Physics and Astronomy Department, Johns Hopkins University, Baltimore, MD 21218, USA; Shawn.Usman@jhu.edu
[2] Harvard-Smithsonian Center for Astrophysics, 60 Garden Street, Cambridge, MA 02138, USA
[3] Department of Physics and Astronomy, Dartmouth College, 6127 Wilder Laboratory, Hanover, NH 03755, USA
[4] Department of Physics and Astronomy, University of Missouri, Kansas City, MO 64110, USA

ABSTRACT

We explore the connection between absorption by neutral gas and extinction by dust in mid-infrared (IR) selected luminous quasars. We use a sample of 33 quasars at redshifts $0.7 < z \lesssim 3$ in the 9 deg^2 Boötes multiwavelength survey field that are selected using *Spitzer Space Telescope* Infrared Array Camera colors and are well-detected as luminous X-ray sources (with >150 counts) in *Chandra* observations. We divide the quasars into dust-obscured and unobscured samples based on their optical to mid-IR color, and measure the neutral hydrogen column density $N_{\rm H}$ through fitting of the X-ray spectra. We find that all subsets of quasars have consistent power law photon indices $\Gamma \approx 1.9$ that are uncorrelated with $N_{\rm H}$. We classify the quasars as gas-absorbed or gas-unabsorbed if $N_{\rm H} > 10^{22}$ cm^{-2} or $N_{\rm H} < 10^{22}$ cm^{-2}, respectively. Of 24 dust-unobscured quasars in the sample, only one shows clear evidence for significant intrinsic $N_{\rm H}$, while 22 have column densities consistent with $N_{\rm H} < 10^{22}$ cm^{-2}. In contrast, of the nine dust-obscured quasars, six show evidence for intrinsic gas absorption, and three are consistent with $N_{\rm H} < 10^{22}$ cm^{-2}. We conclude that dust extinction in IR-selected quasars is strongly correlated with significant gas absorption as determined through X-ray spectral fitting. These results suggest that obscuring gas and dust in quasars are generally co-spatial, and confirm the reliability of simple mid-IR and optical photometric techniques for separating quasars based on obscuration.

Key words: galaxies: active – galaxies: evolution – galaxies: nuclei – infrared: galaxies – quasars: general – X-rays: galaxies

Online-only material: color figures

1. INTRODUCTION

In the past decade, sensitive mid-infrared (IR) observations with the *Spitzer Space Telescope* and *Wide-Field Infrared Explorer* (*WISE*) have forever changed our understanding of black hole (BH) growth by unveiling, at last, large populations of obscured quasars. Many luminous type 2 active galactic nuclei (AGNs) have been identified from narrow optical emission lines (Zakamska et al. 2003, 2004, 2005; Reyes et al. 2008), radio luminosity (e.g., McCarthy 1993; Martínez-Sansigre et al. 2006; Seymour et al. 2007), or X-ray properties (e.g., Alexander et al. 2001; Stern et al. 2002; Treister et al. 2004; Vignali et al. 2006, 2009), but the most efficient techniques for finding obscured quasars employ mid-IR photometry. Pioneering work with *Spitzer* showed that obscured quasars have similar mid-IR spectral energy distributions (SEDs) to their unobscured counterparts, but are dominated by host galaxy light in the optical (Lacy et al. 2004; Stern et al. 2005; Rowan-Robinson et al. 2005; Polletta et al. 2006; Alonso-Herrero et al. 2006; Donley et al. 2008; Hickox et al. 2007, hereafter H07). In the mid-IR, obscured quasars can be reliably selected using simple color criteria, in particular being very red in [3.6]–[4.5] (characteristic of a "hot" mid-IR SED) and very red in $R - [4.5]$, indicating a faint optical counterpart (Figure 1). Mid-IR studies find roughly equal numbers of obscured and unobscured quasars (e.g., H07; Donoso et al. 2014).

Obscured quasars therefore represent a large fraction of the massive BH growth in the universe, but their precise nature remains a mystery. In particular, what is the origin of the obscuring material, and what role do these objects play in the evolution of BHs and galaxies? The simple "unified model" for AGNs attributes obscuration to the orientation of a gas- and dust-rich torus intrinsic to the central engine (e.g., Antonucci 1993; Ballantyne et al. 2006), but it is not clear whether this model applies to objects with quasar luminosities. A competing hypothesis is that quasars are fueled by major mergers of galaxies that drive gas and dust clouds to the nucleus, obscuring the central engine, as suggested in models of BH–galaxy co-evolution (e.g., Sanders et al. 1988; Hopkins et al. 2008).

One clue about the nature of the obscuring material is the connection between obscuration by *dust* which is manifested through extinction of rest-frame ultraviolet and optical nuclear light, and absorption by neutral *gas* which is detectable by its effect on the observed X-ray spectrum. In the simplest unified scenarios, neutral gas and dust are co-spatial and so both types of obscuration should be observed in the same systems. This is in fact what is observed in most obscured AGNs; however, $\sim$30% of moderate-luminosity AGNs show a mismatch between optical and X-ray classification criteria (e.g., Tozzi et al. 2006; Trouille et al. 2009), suggesting some deviation from the simplest unified scenario.

Obscuration is particularly interesting for powerful quasars (given the expected importance of merger fueling) but the obscuration properties of luminous AGNs have been less well studied due to their relative rarity. Furthermore, it is also interesting to study the obscuration in luminous quasars given the reported decreasing trend of obscured AGNs at increasing luminosities (e.g., Ueda et al. 2003; Hasinger et al. 2005; Merloni et al. 2014). A recent study of X-ray selected AGNs in the COSMOS field Merloni et al. (2014) found that at quasar luminosities ($L_X > 10^{44}$ erg s^{-1}) $\sim$80% of AGNs have classifications for dust and gas obscuration that agree, with the majority of the "mismatch"

corresponding to optically unobscured but gas-obscured sources. Previous studies of such objects have suggested they are preferentially hosted by more rapidly star-forming galaxies, indicating that the X-ray absorbing gas arises from galaxy-scale structures that are far larger than the putative torus, and may be associated with an outflowing wind (Page et al. 2004). However, Merloni et al. (2014) found that X-ray obscured, optically un-obscured quasars have spectra and photometric properties that are identical to their X-ray unobscured counterparts, suggesting that the absorption may instead be due to small-scale clouds within the putative torus.

In this study, we further explore the connection between gas and dust obscuration in luminous quasars, using observations from the wide-field (9 deg^2) Boötes multiwavelength survey area that enable efficient selection of rare, luminous sources. We analyze X-ray spectra of 33 high-luminosity IR-selected quasars in the XBoötes Deep Survey. We find a strong correspondence between dust and gas obscuration in luminous quasars, consistent with the predictions of unified models as well as simple evolutionary scenarios in which the gas and dust are co-spatial.

2. OBSERVATIONS AND QUASAR SAMPLE

Our sample of quasars is drawn from H07, who selected 1479 luminous AGNs based on the mid-IR color criteria of Stern et al. (2005). The vast majority of these sources have estimates of bolometric luminosity $L_{bol} > 10^{12} L_{\odot}$ corresponding to the commonly used division between "Seyfert galaxies" and "quasars" (e.g., Hopkins & Hernquist 2009), so for the remainder of this Letter we refer to the sample objects as quasars. The mid-IR observations come from the *Spitzer* Infrared Array Camera Shallow Survey (Eisenhardt et al. 2004; Brodwin et al. 2006) and optical photometry from the NOAO Deep Wide Field Survey Jannuzi & Dey (1999), and is limited to redshifts $0.7 < z < 3$ determined by optical spectroscopy from the AGN and Galaxy Evolution Survey (AGES; Kochanek et al. 2012) or using photometric redshifts from Brodwin et al. (2006). H07 found that the full IR-selected quasar sample could be easily divided into dust-obscured and unobscured sources based on their optical to mid-IR color, as they exhibited a bimodal color distribution with a boundary at $R − [4.5] = 6.1$ (or equivalently $\log(L_R/L_{4.5\,\mu m}) = −0.4$, where L_R and $L_{4.5\,\mu m}$ are the luminosities in the *observed*-frame R and 4.5 μm bands; see Figure 1). We also include estimates of quasar bolometric luminosity derived from fitting mid-IR SEDs, as described by Hickox et al. (2011).

H07 showed that the objects with blue $R − [4.5]$ colors are dominated in the optical by unobscured light from the quasar nucleus, while the nucleus is obscured in the redder sources such that the optical light is dominated by the host galaxy. H07 also showed via an X-ray stacking analysis that the average X-ray spectra of unobscured quasars were consistent with no absorption by neutral gas, while the obscured quasars had harder average X-ray spectra indicating significant gas absorption with $N_H \sim 3 \times 10^{22}$ cm^{-2}. However, given the shallow (5 ks; Murray et al. 2005) X-ray observations available in the H07 analysis, this comparison was only possible for *average* X-ray hardness ratios and could not explore variations in X-ray spectra between individual sources.

This study expands on that work by analyzing deeper *Chandra* ACIS observations (including from the XBoötes Deep Survey) of quasars in the H07 sample. The deeper observations consist of 36 exposures between 2001 and 2012 with an average exposure time of 41.6 ks, of which 13 are with the ACIS-I array and
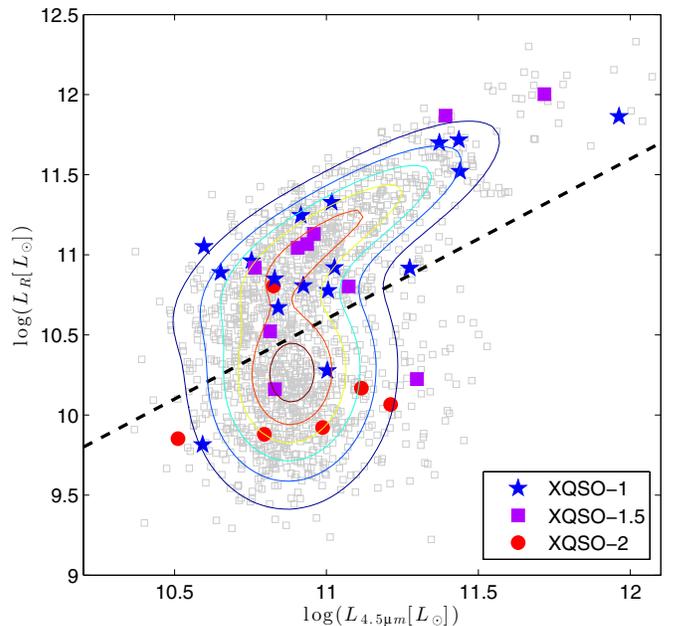

Figure 1. $L_{4.5\,\mu m}$ vs. L_R (calculated as νL_ν in the observed frame) for IR-selected quasars. The selection boundary of $\log(L_R/L_{4.5\,\mu}) = −0.4$ (corresponding to $R − [4.5] = 6.1$ in Vega magnitudes) is shown as a dashed line with IRQSO-1s and IRQSO-2s residing above and below the line, respectively. Contours are derived from IR source density. The filled blue stars (XQSO-1), purple squares (XQSO-1.5), and red circles (XQSO-2) are the X-ray classifications for our X-ray spectroscopic sample, discussed in Section 3.

(A color version of this figure is available in the online journal.)

13 are with ACIS-S (Table 1). The data were reprocessed using the CHAV (version 2011.01.25) and CIAO 4.1.2 (CALDB 4.1.4) packages. To obtain sufficient quality X-ray spectra we limit our analyses to objects with >150 counts in the 0.2–7 keV band. We match the sources to the 1479 IR-selected quasars from H07 using the TOPCAT (Taylor 2005) cone-search algorithm with a 10″ radius. A total of 33 quasars were selected, with an average of ≈300 counts per source.

Using the H07 $R − [4.5]$ color criterion, 24 of the IR-selected quasars in our sample are classified as unobscured (IRQSO-1) while 9 are obscured (IRQSO-2). Our bright X-ray spectroscopic sample contains a low fraction of IRQSO-2s (9/33 or 27%) that is significantly smaller than the 43% obscured fraction in the full IRQSO sample from H07. This is due to the fact that X-ray QSO2s are generally fainter in X-rays; the fraction of IRQSOs with X-ray counterparts in original shallow (5 ks) XBoötes survey is ≈60% for IRQSO-1s and only ≈30% for IRQSO-2s, while the average X-ray flux of the unde-tected sources, determined from stacking, is also systematically lower for the IRQSO-2s (H07). The fainter X-ray emission from IRQSO-2s is most likely due to higher levels of gas obscuration that not only hardens the X-ray spectrum but reduces the observed flux (e.g., Alexander et al. 2008). This fact reflects a correspondence between gas and dust obscuration in these quasars, which we aim to test further by direct measurement of the obscuring column density (N_H) in the X-ray spectra of the bright sources for which these measurements are possible.

3. X-RAY ANALYSIS

We extract source and background spectra and produce response functions using standard CIAO software. Sources and background spectra were extracted from hand-selected

Table 1
Spectral Parameters and X-Ray Classification

Identifier	Exposure (ks)	z^a	Counts (0.5–7 keV)	F_x^b (10^{-14}erg cm^{-2} s^{-1})	log (L_x) (erg s^{-1})	Γ	$N_H \pm 1\sigma^c$ (10^{22} cm^{-2})	XQSO Class
				IRQSO-1				
SDWFS J142942.63+335654.94	47.1	1.1251	607	17.3	45.1	1.77 ± 0.09	0 + 0.07	1
SDWFS J142810.31+353847.31	37.9	0.8028	852	16.5	44.7	1.80 ± 0.07	0 + 0.02	1
SDWFS J143520.20+340929.20	42.6	1.0972	182	1.75	44.1	2.13 ± 0.20	0 + 0.08	1
SDWFS J143520.60+340514.68	42.6	0.7973	217	3.38	44.0	1.59 ± 0.14	0 + 0.06	1
SDWFS J143513.41+350053.77	44.0	1.1471	325	3.50	44.4	1.81 ± 0.13	0 + 0.15	1
SDWFS J143520.14+350413.23	44.0	1.0512	339	1.10	43.8	2.30 ± 0.18	0 + 0.13	1
SDWFS J142922.94+351517.74	42.0	0.9041	408	10.4	44.6	1.87 ± 0.14	0 + 0.09	1
SDWFS J142634.05+351602.56	14.9	1.1055	177	6.61	44.7	1.61 ± 0.17	0 + 0.17	1
SDWFS J143651.98+350537.97	54.3	0.864	200	0.54	43.3	2.49 ± 0.21	0 + 0.05	1
SDWFS J142651.47+351924.40	29.7	1.756	833	12.4	45.4	1.83 ± 0.07	0 + 0.07	1
SDWFS J142839.20+353455.55	37.9	1.0693	228	5.31	44.5	1.70 ± 0.16	0 + 0.35	1
SDWFS J142829.91+342758.68	68.6	1.1401	301	3.31	44.4	1.93 ± 0.16	0 + 0.41	1
SDWFS J143245.88+333758.45	33.8	1.0816	192	3.43	44.3	2.13 ± 0.26	0 + 0.34	1
SDWFS J142917.20+342130.31	28.7	1.2734	306	6.06	44.8	2.07 ± 0.18	0 + 0.56	1
SDWFS J142607.71+340426.61	51.2	4.32	468	7.27	46.1	2.67 ± 0.12	0 + 0.94	1
SDWFS J143310.25+335421.99	27.7	0.8792	238	9.62	44.6	1.79 ± 0.33	0.57 + 0.75	1.5
SDWFS J143153.67+344138.17	50.2	0.8254	481	8.16	44.4	1.72 ± 0.17	1.31 ± 0.30	2
SDWFS J142658.70+324003.78	42.0	1.7737	212	5.45	45.1	1.56 ± 0.25	0 + 1.67	1.5
SDWFS J142915.19+343820.18	29.7	2.3515	202	3.87	45.2	2.12 ± 0.27	0 + 1.83	1.5
SDWFS J142622.68+334202.41	33.8	1.3517	182	4.27	44.7	1.94 ± 0.31	0.42 + 1.41	1.5
SDWFS J143434.40+330549.14	56.8	2.0656	154	0.49	44.2	2.39 ± 0.45	0.76 + 2.38	1.5
SDWFS J142859.55+350349.11	42.0	1.6126	165	2.89	44.7	2.19 ± 0.45	1.28 + 2.21	1.5
SDWFS J143431.07+332825.51	39.9	1.0554	155	4.70	44.5	1.76 ± 0.38	1.45 + 1.68	1.5
SDWFS J143450.01+352520.65	30.7	0.9629	184	8.17	44.6	2.56 ± 0.42	1.98 ± 1.09	1.5
				IRQSO-2				
SDWFS J143210.97+343957.89	81.9	0.83	204	1.93	43.8	1.66 ± 0.24	0 + 0.66	1
SDWFS J142824.97+352842.63	37.9	1.49	217	4.90	44.8	1.98 ± 0.20	0 + 0.71	1
SDWFS J142845.07+350903.30	42.0	0.81	463	9.52	44.5	1.87 ± 0.20	0.72 ± 0.42	1.5
SDWFS J142813.98+325502.82	33.8	1.54	264	10.8	45.2	1.08 ± 0.28	2.21 + 3.35	1.5
SDWFS J143502.04+330556.51	56.8	1.58	299	5.09	44.9	1.84 ± 0.25	3.07 + 1.62	2
SDWFS J143503.49+340241.92	42.6	1.06	219	2.54	44.2	2.85 ± 0.44	3.41 + 1.35	2
SDWFS J143359.09+331301.06	42.0	0.92	330	17.3	44.9	1.64 ± 0.31	3.97 ± 1.49	2
SDWFS J142916.10+335537.36	24.6	0.98	220	7.30	44.6	2.36 ± 0.34	4.34 ± 1.21	2
SDWFS J142707.05+325214.17	42.0	2.28	244	5.65	45.4	1.97 ± 0.28	5.66 ± 2.98	2

Notes.
[a] Differences in redshift precision correspond to the differences between spectroscopic and photometric estimates (Section 2).
[b] Fluxes and luminosities are unabsorbed and calculated in the 0.5–7 keV band.
[c] Entries with plus signs only indicate that the lower bound is equal to zero.

circular regions with mean radii of 11.5 pixels and 100.1 pixels, respectively. The resulting spectra were fit using SHERPA (4.1.2) with a one-dimensional power law (xspowerlaw.p1) convolved with two neutral hydrogen absorption laws, one for the Milky Way (xswabs.abs1), and one for the host galaxy (xszwabs.abs2) absorption. The Milky Way absorption column density was frozen at the mean of all 33 quasars, $N_{H-MW} = 1.05 \times 10^{20}$ cm^{-2}, derived from the *Chandra* X-Ray Center's COLDEN calculator. The host galaxy redshifts are fixed at values taken either from AGES spectroscopic measurements (Kochanek et al. 2012) or photometric redshifts (Brodwin et al. 2006), as described in H07. The power-law index Γ, normalization, and intrinsic N_H were allowed to vary in the spectral fitting. Examples of the X-ray spectral fits are shown in Figure 2 for one source showing no evidence for gas absorption, and another with detectable N_H.

The spectral fit parameters (Γ and intrinsic N_H) and 1σ errors along with other quasar properties are shown in Table 1. In many cases, the observed N_H is consistent with zero and only upper limits are obtained. We classify the quasars as gas-absorbed

(XQSO-2) or gas-unabsorbed (XQSO-1) if $N_H > 10^{22}$ cm^{-2} or $N_H < 10^{22}$ cm^{-2}, respectively, following the convention used widely in the literature (e.g., Tozzi et al. 2006; Lanzuisi et al. 2013; Ueda et al. 2014). For several sources (XQSO-1.5) the classification is ambiguous, with N_H consistent with either subset within the uncertainties. (We note that a division at $N_H = 10^{21.5}$ cm^{-2}, as in Merloni et al. 2014, produces more ambiguous classifications due to the uncertainties in our N_H measurements, but results in the same qualitative conclusions.) In Figure 1 we show the IR and optical luminosities of the quasars in different X-ray classes, and in Figure 3 we show the distribution in Γ and N_H for all the sources. We note that there is no clear correlation between Γ and N_H, verifying that we have sufficient counts in each source to sufficiently break the degeneracy between those parameters. The error-weighted average value of Γ is 1.89 ± 0.03 for the full sample, and for the subsets is 1.90 ± 0.03 (XQSO-1), 1.83 ± 0.10 (XQSO-1.5) and 1.90 ± 0.11 (XQSO-2), all consistent with previous measurements for the intrinsic photon index for AGNs and quasars (e.g., Tozzi et al. 2006; Xue et al. 2011).
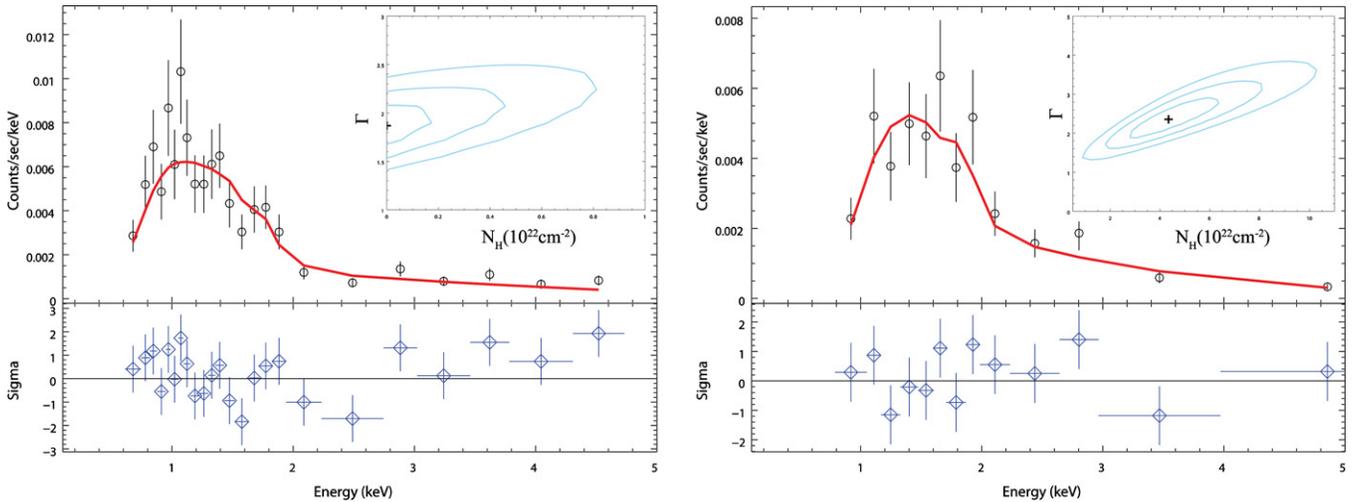
Figure 2. (a) X-ray spectrum with best-fit model a gas-unobscured XQSO-1. Contours of N_H vs. Γ are shown in the subset. (b) Same as (a), but for a gas-obscured XQSO-2. A clear cut-off in spectra for energies <1 keV is absent in the XQSO-1 (a), but observed in the XQSO-2 (b).

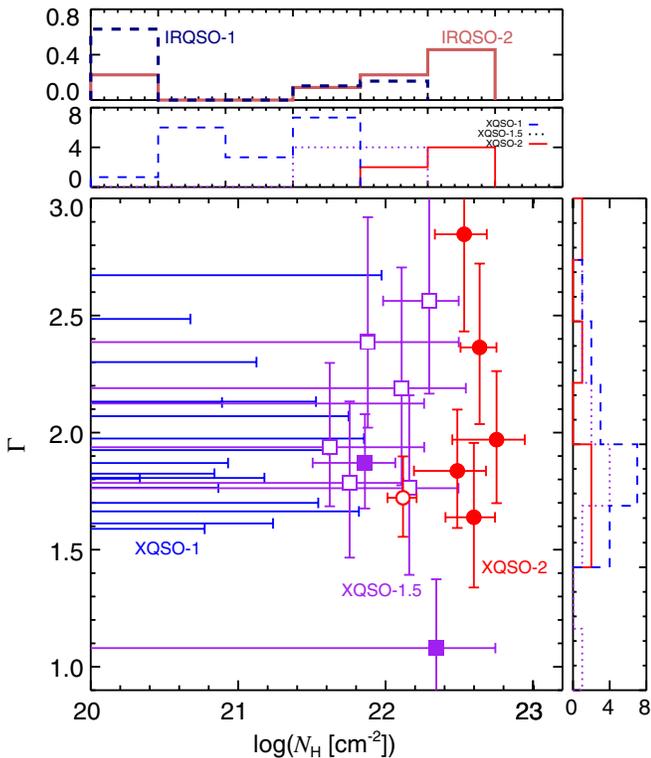(A color version of this figure is available in the online journal.)

Figure 3. X-ray spectral fit parameters for the full sample of 33 IR- and X-ray selected quasars. The main panel shows Γ and N_H with uncertainties, highlighting the population of XQSO-1.5s with ambiguous classifications, and showing that there is no clear correlation between Γ and N_H. Dust unobscured (IRQSO-1) sources are marked with open symbols. The top panel shows the fractional distribution of the best-fit values of N_H for the IRQSO-1s and 2s, respectively, showing the clear correlation between dust and gas obscuration. The other two panels show the distributions in best-fit N_H and Γ for the XQSO-1s, 1.5s, and 2s separately.

(A color version of this figure is available in the online journal.)

The primary result of this analysis is the correspondence between the optical/mid-IR and X-ray obscuration criteria. Among the 24 dust-unobscured (IRQSO-1) quasars, we find 15 XQSO-1s, 8 XQSO-1.5s (of which 7 have N_H consistent with zero), and only one XQSO-2. In contrast, the 9 dust-obscured

quasars (IRQSO-2s) comprise only 2 XQSO-1s, 2 XQSO-1.5s (of which one has N_H consistent with zero) and 5 XQSO 2s. We thus obtain a strong, if not perfect, correlation between absorption by gas and dust, with only a few examples showing clearly anomalous gas absorption for the observed optical and mid-IR properties (broadly consistent with the results of Merloni et al. 2014. The largest N_H observed in our XQSO-2 sample is relatively modest (only a few $\times 10^{22}$ cm^{-2}); it is likely that more heavily obscured sources ($N_H > 10^{23}$) are excluded from our X-ray spectroscopic sample because their observed fluxes are too faint to yield the required numbers of counts, as discussed in Section 2.

4. DISCUSSION AND CONCLUSIONS

Overall, these results indicate that obscuration by gas and dust are strongly correlated in IR-selected luminous quasars. This correspondence indicates that gas and dust obscuration generally arise in the same structures, consistent with the predictions of the unified model but also with the simplest evolutionary models. We thus cannot draw robust conclusions about whether the obscuring material is in a small-scale torus or due to larger-scale galactic structures. A recent study of their far-IR properties using 250 μm data from *Herschel* suggests that the IRQSO-2s have higher average rates of star formation than IRQSO-1s (C.-T. Chen et al. 2014, in preparation), suggesting that at least some quasars are obscured by galaxy-scale material associated with rapid star formation. However, only 4 of our 33 objects are detected at 250 μm with *Herschel* and of these two show neither gas nor dust obscuration, while the other two are obscured in both classifications, so it is unclear whether large-scale material is responsible for any of the observed obscuration.

We find that only a small fraction of dust-unobscured quasars show *clear* X-ray absorption signatures. Of the quasars in our X-ray spectroscopic sample, $\approx 17\%$ are IRQSO-1s with best-fit values of $N_H > 10^{22}$ cm^{-2}, similar to the fraction of such mismatches found by Merloni et al. (2014). We note however that all but one of these objects are consistent with having little or no gas absorption, and their distribution in the plane IR and optical luminosity (Figure 1) is indistinguishable to IRQSO-1s with no X-ray absorption. We therefore caution that the observed incidence of these mismatches must be treated as an upper limit,

and that the X-ray absorbed broad-line quasars may in fact be rare in the full quasar population; an accurate census of quasars with modest obscuration provides strong motivation for future high-throughput X-ray observatories.

Overall our results serve to verify that obscured quasar selection based on optical to mid-IR color H07 preferentially identifies systems that show evidence for obscuration at other wavelengths. Even in our bright X-ray spectroscopic sample, for which the effective flux limit biases us *against* heavily X-ray obscured sources as discussed in Section 2, we still find that the majority of dust-obscured quasar candidates show clear evidence for X-ray absorption. This indicates that the full population of dust-obscured quasars likely has a very high incidence of corresponding gas absorption. These results confirm that optical/mid-IR color selection is effective in selecting even moderately obscured quasars at the highest luminosities, providing a strong basis for future large statistical studies of obscured quasars selected based on *WISE* and optical photometry.

Facilities: CXO (ACIS), *Spitzer*, Mayall (MOSAIC-1)

REFERENCES

Alexander, D. M., Brandt, W. N., Hornschemeier, A. E., et al. 2001, AJ, 122, 2156
Alexander, D. M., Chary, R.-R., Pope, A., et al. 2008, ApJ, 687, 835
Alonso-Herrero, A., Pérez-González, P. G., Alexander, D. M., et al. 2006, ApJ, 640, 167
Antonucci, R. 1993, ARA&A, 31, 473
Ballantyne, D. R., Shi, Y., Rieke, G. H., et al. 2006, ApJ, 653, 1070
Brodwin, M., Brown, M. J. I., Ashby, M. L. N., et al. 2006, ApJ, 651, 791
Donley, J. L., Rieke, G. H., Pérez-González, P. G., & Barro, G. 2008, ApJ, 687, 111
Donoso, E., Yan, L., Stern, D., & Assef, R. J. 2014, ApJ, in press (arXiv:1309.2277)
Eisenhardt, P. R., Stern, D., Brodwin, M., et al. 2004, ApJS, 154, 48
Hasinger, G., Miyaji, T., & Schmidt, M. 2005, A&A, 441, 417
Hickox, R. C., Jones, C., Forman, W. R., et al. 2007, ApJ, 671, 1365
Hickox, R. C., Myers, A. D., Brodwin, M., et al. 2011, ApJ, 731, 117
Hopkins, P. F., & Hernquist, L. 2009, ApJ, 694, 599
Hopkins, P. F., Hernquist, L., Cox, T. J., & Kereš, D. 2008, ApJS, 175, 356
Jannuzi, B. T., & Dey, A. 1999, in ASP Conf. Ser. 191, Photometric Redshifts and the Detection of High Redshift Galaxies, ed. R. Weymann et al. (San Francisco, CA: ASP), 111
Kochanek, C. S., Eisenstein, D. J., Cool, R. J., et al. 2012, ApJS, 200, 8
Lacy, M., Storrie-Lombardi, L. J., Sajina, A., et al. 2004, ApJS, 154, 166
Lanzuisi, G., Civano, F., Elvis, M., et al. 2013, MNRAS, 431, 978
Martínez-Sansigre, A., Rawlings, S., Lacy, M., et al. 2006, MNRAS, 370, 1479
McCarthy, P. J. 1993, ARA&A, 31, 639
Merloni, A., Bongiorno, A., Brusa, M., et al. 2014, MNRAS, 437, 3550
Murray, S. S., Kenter, A., Forman, W. R., et al. 2005, ApJS, 161, 1
Page, M. J., Stevens, J. A., Ivison, R. J., & Carrera, F. J. 2004, ApJL, 611, L85
Polletta, M. d. C., Wilkes, B. J., Siana, B., et al. 2006, ApJ, 642, 673
Reyes, R., Zakamska, N. L., Strauss, M. A., et al. 2008, AJ, 136, 2373
Rowan-Robinson, M., Babbedge, T., Surace, J., et al. 2005, AJ, 129, 1183
Sanders, D. B., Soifer, B. T., Elias, J. H., et al. 1988, ApJ, 325, 74
Seymour, N., Stern, D., De Breuck, C., et al. 2007, ApJS, 171, 353
Stern, D., Eisenhardt, P., Gorjian, V., et al. 2005, ApJ, 631, 163
Stern, D., Moran, E. C., Coil, A. L., et al. 2002, ApJ, 568, 71
Taylor, M. B. 2005, in ASP Conf. Ser. 347, Astronomical Data Analysis Software and Systems XIV, ed. P. Shopbell, M. Britton, & R. Ebert (San Francisco, CA: ASP), 29
Tozzi, P., Gilli, R., Mainieri, V., et al. 2006, A&A, 451, 457
Treister, E., Urry, C. M., Chatzichristou, E., et al. 2004, ApJ, 616, 123
Trouille, L., Barger, A. J., Cowie, L. L., Yang, Y., & Mushotzky, R. F. 2009, ApJ, 703, 2160
Ueda, Y., Akiyama, M., Hasinger, G., Miyaji, T., & Watson, M. G. 2014, ApJ, 786, 104
Ueda, Y., Akiyama, M., Ohta, K., & Miyaji, T. 2003, ApJ, 598, 886
Vignali, C., Alexander, D. M., & Comastri, A. 2006, MNRAS, 373, 321
Vignali, C., Pozzi, F., Fritz, J., et al. 2009, MNRAS, 395, 2189
Xue, Y. Q., Luo, B., Brandt, W. N., et al. 2011, ApJS, 195, 10
Zakamska, N. L., Schmidt, G. D., Smith, P. S., et al. 2005, AJ, 129, 1212
Zakamska, N. L., Strauss, M. A., Heckman, T. M., Ivezić, Ž., & Krolik, J. H. 2004, AJ, 128, 1002
Zakamska, N. L., Strauss, M. A., Krolik, J. H., et al. 2003, AJ, 126, 2125